SCIENCE CHINA
Physics, Mechanics & Astronomy

• Article •

December 2014 Vol. 57 No. 12: 2297–2308
doi: 10.1007/s11433-014-5605-z

Simulation of triaxial response of granular materials by modified DEM

WANG XiaoLiang* & LI JiaChun*

Key Laboratory for Mechanics in Fluid Solid Systems, Institute of Mechanics, Chinese Academy of Sciences, Beijing 100190, China

Received January 21, 2014; accepted September 5, 2014; published online October 14, 2014

A modified discrete element method (DEM) with rolling effect taken into consideration is developed to examine macroscopic behavior of granular materials in this study. Dimensional analysis is firstly performed to establish the relationship between macroscopic mechanical behavior, mesoscale contact parameters at particle level and external loading rate. It is found that only four dimensionless parameters may govern the macroscopic mechanical behavior in bulk. The numerical triaxial apparatus was used to study their influence on the mechanical behavior of granular materials. The parametric study indicates that Poisson's ratio only varies with stiffness ratio, while Young's modulus is proportional to contact modulus and grows with stiffness ratio, both of which agree with the micromechanical model. The peak friction angle is dependent on both inter-particle friction angle and rolling resistance. The dilatancy angle relies on inter-particle friction angle if rolling stiffness coefficient is sufficiently large. Finally, we have recommended a calibration procedure for cohesionless soil, which was at once applied to the simulation of Chende sand using a series of triaxial compression tests. The responses of DEM model are shown in quantitative agreement with experiments. In addition, stress-strain response of triaxial extension was also obtained by numerical triaxial extension tests.

granular materials, rolling resistance, DEM, calibration, YADE

PACS number(s): 45.70.Cc, 81.05.Rm, 62.20.de, 62.20.dj

Citation: Wang X L, Li J C. Simulation of triaxial response of granular materials by modified DEM. Sci China-Phys Mech Astron, 2014, 57: 2297–2308, doi: 10.1007/s11433-014-5605-z

1 Introduction

Granular materials, composed of an assemblage of particles or blocks, are ubiquitous in nature and industry. Mechanical behavior of granular materials depends on many factors, such as macroscopic packing density, stress state, stress history etc. and microscopic average coordination number, grain size distribution, grain shape/roughness, force chains, fabric etc. The study of mechanical behavior of granular materials is considerably significant in natural hazards forecast, for example, in answering whether a slope might be firm enough or not, especially after a heavy rain [1,2]. Sand and gravel classified as cohesionless soil are two typical granular materials. Despite the great success achieved by the elasto-plastic constitutive modeling, there are still challenging issues in granular materials study, which probably can be handled by DEM [3] from the angle of particle mechanics model.

Numerical algorithms in contact detection technique and contact physics for spherical particles [3], ellipsoid particles [4], clump of particles [5] and polyhedral particles [6] have advanced rapidly in recent decades. DEM has found its applications in both fundamental research and engineering applications in soil mechanics [7–15]. For example, Ji [7] studied probability of contact forces in quasi-solid-liquid

*Corresponding author (LI JiaChun, email: jcli05@imech.ac.cn; WANG XiaoLiang, email: wangxiaoLiang52086@126.com)

phase transition of granular shear flow. Thornton [9] used 3D DEM to study strain response during stress loading in deviatoric stress space. Wang et al. [11], Utili et al. [12] and Jiang et al. [13,14] used DEM to study the shear behavior, strain localization, yielding behavior, etc. of bonded granular geomaterials. However, when DEM is applied to real granular materials, there are a lot of bottlenecks such as capabilities of computer, efficient contact models, treatment of complex grain shape/roughness, and coupling between particles and liquid, etc. So it is almost infeasible for original DEM to model real granular materials in order to capture all the mechanical properties including strength and dilatancy.

Non-spherical particles of a real granular material, either sand or gravel, generally transmit moment by rolling over each other [16]. Since spherical particles obviously roll much easier than non-spherical particles, spherical particle model generally underestimates friction angle and overestimates dilatancy angle of the packing [17]. Salot et al. [5] have used clump particles by aggregating spherical particles together, with two parameters considered to cope with the non-spherical effect, i.e. angularity coefficient and slavery number of a clump. Although he succeeded in modeling triaxial compression of Ticino sand, his calibration involves strong couple between two non-spherical parameters and mechanical properties of the packing. Ng [4] developed ellipsoid shape particle model. Mollon and Zhao [18] modeled the particle morphology using Fourier analysis of real particle. The above two techniques enhance DEM capability to simulate behavior of granular material much closer to real granular materials than original DEM, but as for real granular materials, it is still challenging. For example, the particle may wear or crush during loading.

Alternatively, we may add a rolling resistance between contacting spherical particles to model non-spherical and surface roughness effect, which is proved computationally efficient. Along this line, people can add a rolling stiffness and sometimes a threshold for plastic moment. Iwashita and Oda [19–21] are the pioneers to introduce the rolling effect into classical DEM to examine the development of shear band during biaxial compression. Jiang et al. [22] made a modification in the rolling stiffness by analyzing rotation between two contacting particles in detail and incorporated it into the house DEM code NS2D. Wang and Zhou [23] developed 2D DEM code with rolling resistance and applied it to the study of localization of granular materials. Later, researchers moved on to incorporate the rolling effect into 3D code to deal with rolling effects. Belheine and Plassiard et al. [24,25] proposed a 3D DEM model considering rolling effect and stated that both rolling resistance and particle friction angle can enhance the strength of the packing, whereas only particle friction angle governs the dilatancy angle. They then used their 3D model to predict the mechanical behavior of Labenne sand. This kind of rolling type DEM is suitable for cohesionless granular materials, like sand and gravel. Later Duriez et al. [26] extended them to model shearing behavior and constitutive relationship of in-filled rock joints.

Furthermore, Scholtès et al. [27] also applied this model to cohesive materials by adding cohesion in between particles to analyze the scale effects of coal strength. Estrada and Taboada et al. [28] have made a series of tests to investigate the role of friction angle and rolling resistance to the strength of granular packing by 2D contact dynamics. Although their 2D results showed that there are three zones, called rolling phase (only friction angle plays a role), transition phase (both friction angle and rolling resistance play a role) and sliding phase (only rolling resistance plays a role) in their paper, the dependence of rolling resistance on dilatancy angle hasn't been entirely clarified. With the power of today's supercomputers, spherical particle model with rolling resistance is a promising scheme to model cohesionless and cohesive real granular materials. With the inclusion of rolling resistance, internal friction angle grows. Dilatancy angle sometimes rises, and sometimes keeps constant. Whether initial Young's modulus depends on rolling resistance is also a question. Since different rolling resistance models involve a different number of parameters, for example, Yade [29] has two, and Jiang's model [22] has only one. So much more detailed tests are needed to derive the relationship between macroscopic and microscopic behaviors in a DEM with rolling resistance model. Especially, there is a need to develop an efficient rolling resistance model for real granular materials.

Therefore, we developed a modified DEM model with rolling resistance for real granular materials based on numerical triaxial test concept in the current article. Using dimensional analysis and numerical simulations, the relationship between microscopic parameters and macroscopic behavior was derived. A calibration procedure is recommended for Chende sand [30], based on which triaxial compression and extension tests were carried out and compared with experiments.

2 Discrete element method and numerical triaxial apparatus

Discrete element method (DEM), invented by Cundall et al. [3] in 1979 for soil, considers soil as an assemblage of solid grains, the translational and rotational motions of which are solved numerically. The mechanical quantities, stress and strain, are statistically determined over some representative volume element (RVE) containing enough number of grains via homogenization techniques [31] or equivalently obtained through the motion and supporting force at the walls, but all of the macroscopic data in this paper are obtained using the latter method. Despite the widely used commercial software PFC3D [32], there are several open source software packages, for example YADE [33] and Esys-

Particle [34]. All of the computations in this study are based on the platform of YADE. YADE [29] is a three dimensional DEM code written by C++ language with a python interface to implement both data and control functions. Several contact laws, initial sample generation functions, boundary schemes and two kinds of particle shapes are provided by YADE, which can be arranged and called in a python script very conveniently. Besides, all the source codes are open to users for revision for their own purpose. However, PFC3D [32] still has a number of limitations to be overcome in later studies.

2.1 Contact laws

Considering two particles with radii of R_1 and R_2 in contact, the contact force can be decomposed into a normal component F_n and a shear component F_s. The normal stiffness and shear stiffness are denoted by k_n and k_s, respectively. So the forces are calculated as shown in eqs. (1) and (2):

$$F_n = k_n U_n, \tag{1}$$

$$\Delta F_s = -k_s \Delta U_s, \tag{2}$$

where U_n is the normal overlapping distance of two contacting spheres. ΔU_s is the incremental tangential displacement. And shear force is calculated by $F_s = \sum \Delta F_s$. If the tangential force exceeds the threshold value of $\mu \| F_n \|_T$, then it is set as $\mu \| F_n \|_T$, where μ is the friction coefficient. In this paper μ equals tan(ϕ), where ϕ is the particle friction angle.

In order to model the moment transmitted by non-spherical particle when it is rotating, a rolling spring is introduced for spherical particle model. Moment transmitted due to rolling is shown in eq. (3):

$$M = k_r \cdot \theta_r, \tag{3}$$

where M is the moment transmitted, k_r is the rolling stiffness, and θ_r is the relative rotation angle between two contacting particles.

In YADE, k_n and k_s are defined alternatively to deal with the size effects in eqs. (4) and (5), so that one can conduct triaxial compression test at a coarser size level [35] in order to reduce computation time.

$$k_n = 2\frac{Y \cdot R_1 \cdot R_2}{(R_1 + R_2)}, \tag{4}$$

$$k_s = \alpha k_n, \tag{5}$$

where Y is the contact Young's modulus, and α is the ratio of shearing stiffness to normal stiffness.

Rolling stiffness is scaled by α_r as shown in eq. (6):

$$k_r = \alpha_r \cdot R_1 \cdot R_2 \cdot k_s. \tag{6}$$

Some rolling resistance models have a plastic threshold value to simulate the plasticity or crush of particles. Actually, YADE's rolling resistance model also has two independent parameters: one is for rolling stiffness, and the other for rolling threshold. With the inclusion of two parameters, there is strong coupling of their influences on both internal friction angle and dilatancy angle, some of which are even contradictory in the literature [22,24,25,28]. In this paper, we are simulating a kind of medium-dense granular material which exhibits only a slight softening process during triaxial compression. And thus, we have set the threshold large enough to avoid its influences.

No dashpot is present in the original contact in YADE, and global damping is used to dissipate the kinematic energy to simulate the quasi-static state. Global damping is realized by adding a damping force contrary to the product of contact force and velocity with a damping coefficient. The damping scheme for rotation motion is similar. Half of the minimum time taken by the wave transferred across the smallest particle is used as the global time step for integration [29]. Detailed DEM aspects of YADE can be found in documents and the source code of YADE [29].

2.2 Numerical triaxial apparatus

Based on the above modified DEM, a numerical triaxial apparatus proposed by the authors is created for triaxial compression and extension tests to explore its feasibility for granular materials consisting of coarser particles in ref. [36]. Firstly, six frictionless plates parallel to the three axes were set up to form a cell for compression as shown in Figure 1(a). Secondly, a numerical granular sample consisting of real size particles is generated in the cell using the makeCloud function in YADE [29]. The mechanical behavior of a granular packing depends on Coordination number, anisotropy of the contact network and homogeneity of the sample [37,38]. It is difficult to generate a sample satisfying all the information. The issue is still a hot topic now in the forum of YADE. For real granular material, we only know the porosity, grain size distribution without information of coordination number, anisotropy of contact network. In this paper, we generated a sample by keeping the same porosity as that in reality. As a matter of experience, a simple and robust radius expansion method, first introduced in PFC and named by Jiang [39], and used by other researchers, such as Chareyre [40], with only little boundary effect close to the wall, is used to generate the initial sample in this study. After that, the sample is isotropically consolidated to a specified confining stress. At this stage, the sample is ready to undergo triaxial compression by moving two vertical plates towards the center of packing, while keeping the lateral stress constant via servo mechanism [17,29]. The servo mechanism is realized by applying the wall velocity artificially to adjust a wall stress close to the target wall stress, together with a wall stress damping process [29]. In the

process, stresses are obtained by dividing the resultant force on the wall over the related area of the specimen, and the strain could be determined by the relative displacement of the wall.

Particle size distribution (psd) and the initial sample under confining stress of 100 kPa are shown in Figure 1. In the sample generation process, rolling resistance is turned off to avoid rolling resistance complexity [41]. Only particle friction angle controls the initial porosity. In this article, a friction angle of 20° is used to generate a target porosity of about 0.40 to model Chende sand [30], which is used as the initial sample in the whole article, if not specially stated. After that, the sample is isotropically consolidated to the specified confining stress for shearing.

If we turn off the rolling resistance and set Y and α as 100 MPa and 0.1, a series of triaxial compression tests with different inter-particle friction angles ϕ such as 20°, 30°, 40°, 50° and 85° are simulated. The responses of the DEM simulation without rolling resistance are shown in Figure 2, which qualitatively captures most fundamental behavior of granular material, but not quantitatively.

2.3 Calibration of microscopic parameters

In Figure 2, the peak internal friction angle and dilatancy angle are calculated for the five different inter-particle angles, and results indicate that a 50° inter-particle friction angle only makes a 30° peak friction angle and a dilatancy angle of about 32.5°. In the experiment under lateral pressure of 100 kPa [30], peak friction angle is about 36°, and dilatancy angle is 12.8°. So the rolling effect is significant. For the sake of simplicity, the moment effect due to non-spherical shape and particle surface roughness, is represented by a rolling spring.

When a real granular material is simulated, the microscopic parameters have to be adjusted to match realistic macroscopic behaviors. For example, by using microscopic parameters in Table 1 for Chende sand, the response of a triaxial compression test of lateral stress 100 kPa is shown in Figure 3. The results of DEM simulation agrees well with the experiments by Li [30]. So the original contact model incorporating rolling resistance may be capable of capturing the main response of real granular materials. Based on this

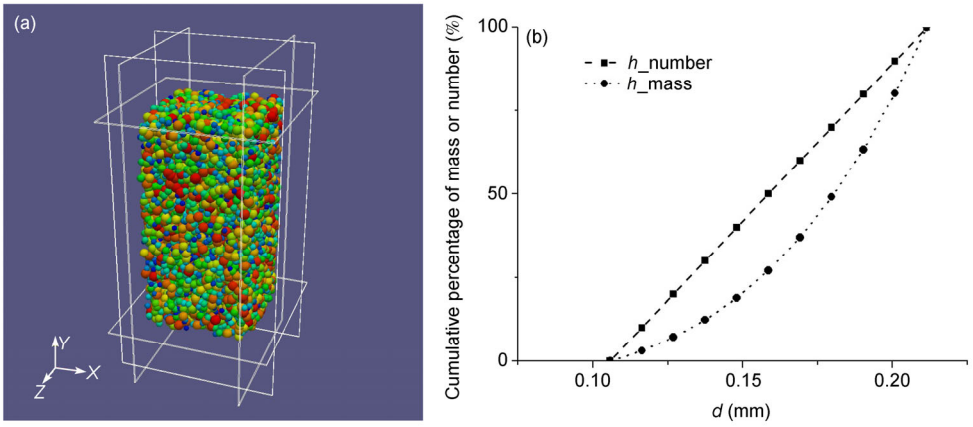

Figure 1 (Color online) Initial granular packing sample under confining stress of 100 kPa and particle size distribution. (a) Initial granular packing; (b) particle size distribution, the line with solid squares denotes cumulative percentage of numbers versus diameter, and the line with solid circles denotes cumulative percentage of mass versus diameter.

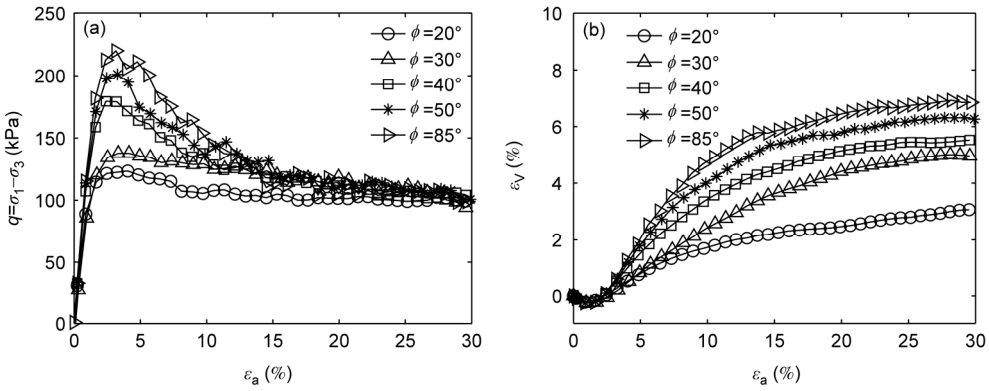

Figure 2 Triaxial compression tests for five different inter-particle friction angles simulated by the DEM model without rolling resistance. (a) Stress versus strain curves; (b) volume strain versus axial strain curves.

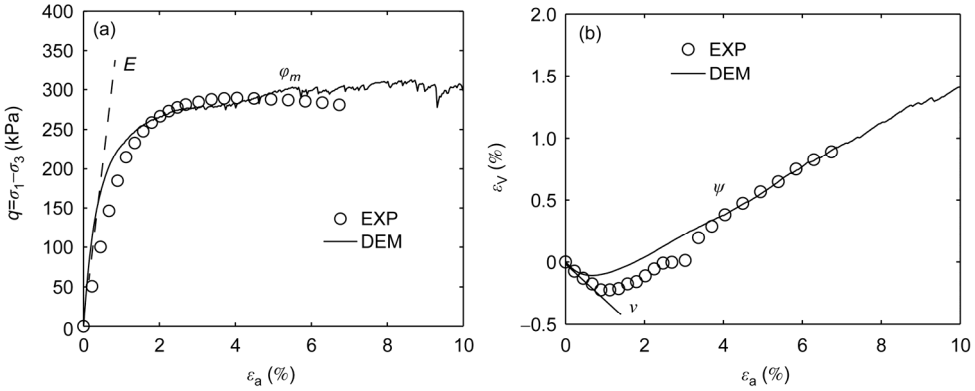

Figure 3 Comparison of DEM triaxial compression simulations with rolling resistance in Table 1 withe experiments: (a) Stress versus strain curve; (b) volume strain versus axial strain curve. E and φ_m in (a) are Young's modulus and friction angle of the granular sample, while ν and ψ in (b) are Poisson's ratio and dilatancy angle.

Table 1 Parameters of the rolling resistance model

Item	Value
Contact Young's modulus Y (MPa)	800
Stiffness ratio α	0.1
Particle friction angle ϕ	22
Coefficient of rolling stiffness α_r	0.6

adjustment, both intrinsic and external influences on the macroscopic behavior are examined later in this study.

3 Dimensional analysis of granular materials in quasi-static state

Stress-strain response and dilatancy shown in Figure 3 demonstrate that mechanical behaviors of a granular material in bulk including initial Young's modulus E, Poisson's ratio ν, friction angle φ_m and the dilatancy angle ψ as shown in Figure 3, are much more complicated than metal. But a lot of factors such as particle density ρ, average radius R, particle size distribution (psd), contact Young's modulus Y, stiffness ratio α, inter-particle friction angle ϕ, the parameters of rolling effect α_r, and those external parameters of the triaxial apparatus, confining stress σ_r, load rate $\dot{\varepsilon}$ and characteristic size of the box H, govern the mechanical behavior of the packing in a triaxial compression test. Dimensional analysis [42] is used here to establish their relationships.

If Z is any one of the macroscopic mechanical parameter shown in Figure 3, Z should be a function of all the factors aforementioned as in eq. (7):

$$Z = f(Y, \alpha, \rho, \phi, \alpha_r, R, psd, \sigma_r, \dot{\varepsilon}, H). \tag{7}$$

If σ_r, R and ρ are chosen as fundamental quantities, eight dimensionless quantities are obtained, and thus eq. (7) can be written into the dimensionless form:

$$Z' = f\left(\frac{Y}{\sigma_r}, \alpha, \phi, \alpha_r, psd, \dot{\varepsilon}R\sqrt{\rho/\sigma_r}, \frac{R}{H}\right), \tag{8}$$

where Z' is the dimensionless number of Z.

Y/σ_r is the stiffness number [38], whose reciprocal governs the ratio between normal deformation of a particle to the size of a particle.

$I = \dot{\varepsilon}\sqrt{\rho R^2/\sigma_r}$ is the inertial number [43,44], the physical meaning of which is the ratio of time scale of particle rearrangement to the time scale of packing shear. In quasi-static problems, it should be as small as 10^{-9} in a real triaxial compression test. However, we can't afford computation time if I is as small as that in the real world. A series of tests with inertial numbers were conducted, and the responses are shown in Figure 4, indicating that if I is as small as 10^{-3}, the response of granular materials does not quite differ from one for larger inertial number I. The result is very close to that in 2D simulation [17]. Hence, the loading rate is chosen 7.3 s^{-1} in all of our simulations with confining stresses 100, 300 and 500 kPa, and particle density 2600 kg/m^3 and radius about 0.09 mm. So I is never larger than 1.0×10^{-4}.

R/H is the ratio of characteristic size between particles and the box. A series of triaxial tests with 1000, 5000, 10000 and 20000 particles were simulated to test the influence of particle size effect. As shown in Figure 5, a sample of 10000 particles could be an appropriate representative volume element. So in order to reduce the computation time, 10000 particles are placed in our box as many authors did when using YADE [24,25,35].

psd represents the particle size distribution [37], which is also remarkably important to the behavior in bulk of the packing. For reducing the CPU time, a uniform distribution is chosen as shown in Figure 1.

Now, the eight dimensionless numbers can be reduced to four, namely, stiffness ratio α, stiffness number Y/σ_r,

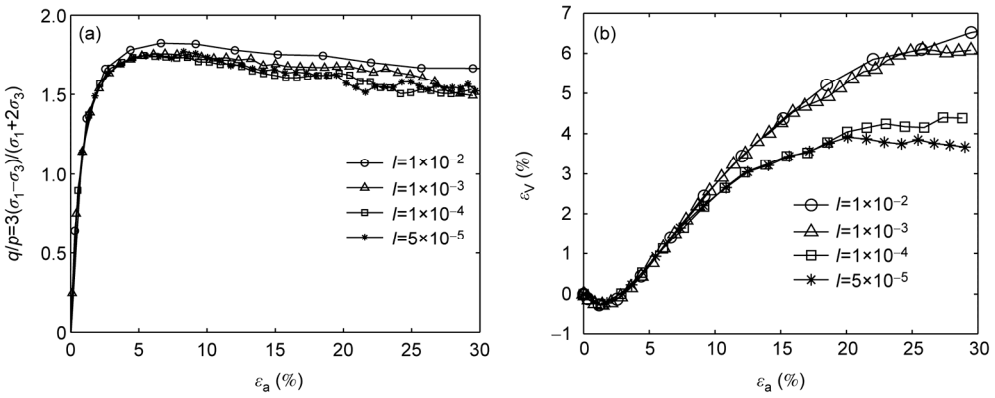

Figure 4 Influence of the inertial number on the response of Chende sand. (a) Stress versus strain response; (b) volume strain versus axial strain response.

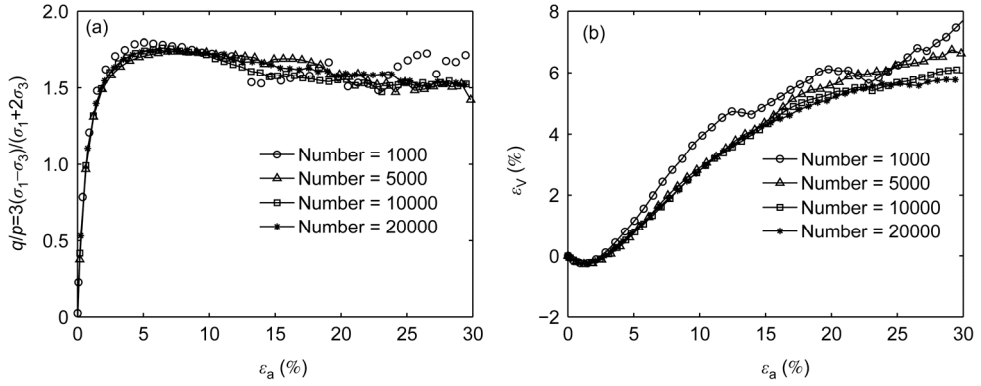

Figure 5 Influence of the number of particles on the response of Chende sand. (a) Stress versus strain response; (b) volume strain versus axial strain response.

particle friction angle ϕ, and the rolling stiffness α_r. As a result, the four mechanical parameters in bulk could be written as function of these four dimensionless numbers from eq. (9) to eq. (12):

$$\frac{E}{Y}=f\left(\frac{Y}{\sigma_r},\alpha,\phi,\alpha_r\right), \tag{9}$$

$$\nu=f\left(\frac{Y}{\sigma_r},\alpha,\phi,\alpha_r\right), \tag{10}$$

$$\varphi_m=f\left(\frac{Y}{\sigma_r},\alpha,\phi,\alpha_r\right), \tag{11}$$

$$\psi=f\left(\frac{Y}{\sigma_r},\alpha,\phi,\alpha_r\right). \tag{12}$$

It is the right mission of micromechanics [45,46] to determine the analytical formulae of the above four equations. However, only the theoretical study for elastic regime and sphere packing interaction without a rolling moment is a mature thus far [45]. So the influence of the four dimensionless parameters on the bulk behavior should be determined numerically through a series of numerical triaxial compression tests.

4 Influence of the four dimensionless number

4.1 Influence of the stiffness number

Most of the micromechanical models show that elastic behavior is only controlled by packing structure, normal and shear stiffness [45,47]. Since no micromechanical model is found for granular packing with a rolling resistance, Chang's micromechanical model [45,47] is referred to. For random distributed sphere packing, the Young's modulus in bulk and Poisson's ratio are shown in eqs. (13) and (14) under a static hypothesis, in which D is the mean diameter of the packing, N_0 is the number of contacts in unit volume, while other parameters are the same as stated above.

$$E=\frac{5k_nN_0D^2\alpha}{3(2+3\alpha)}, \tag{13}$$

$$\nu=\frac{1-\alpha}{(2+3\alpha)}. \tag{14}$$

A series of tests with different stiffness numbers are per-

formed. The Young's modulus of the packing increases with contact modulus, but by scaling with contact modulus Y, the dimensionless Young's modulus does not vary with stiffness number if it is larger than 2000, as shown in Figure 6.

The results show that Young's modulus is proportional to contact modulus, and Poisson's ratio is independent of contact modulus, which is in agreement with Chang's micromechanical model. 2000 for the stiffness number seems to be sufficient for the overlaps of all the particles small enough compared to the particle size, which coincides with the small deformation hypothesis made in Chang's micromechanical model [45].

4.2 Influence of the stiffness ratio

With Y set as 800 MPa, four values of stiffness ratio were tested. It is found in Figure 7 that the trends of our DEM simulation for dimensionless Young's modulus and Poisson's ratio versus α are not the same, but close to Chang's micromechanical model. Namely, the Young's modulus increases with α, whereas the Poisson's ratio decreases with α.

A large α represents high ability of tangential deformation resistance for particles in contact, and the resemble effect is to decrease the lateral deformation for the same axial deformation, so Poisson's ratio is lower. The resistance in lateral generates more stable force network in the axial direction, which makes the sample stiffer in the axial direction. All these simulation results coincide with Chang's micromechanical model as shown in Figure 7.

4.3 Influence of the particle friction angle

Friction angle between particles is a physical parameter dependent on the mineral, water content and chemical composition etc and very hard to measure. Mitchell [16] collected some friction angles between different mineral surfaces, while Li [48] listed some friction angles between different minerals. The information about friction angle between different minerals is shown in Table 2, which is a summary of data from books of Mitchell [16] and Li [48]. Cohesionless mineral has a larger friction angle than cohesive mineral, but they are never larger than 40°. By changing the particle friction with fixed $Y/\sigma_r = 2700$, four tests of Chende sand were performed and shown in Figure 8. It is

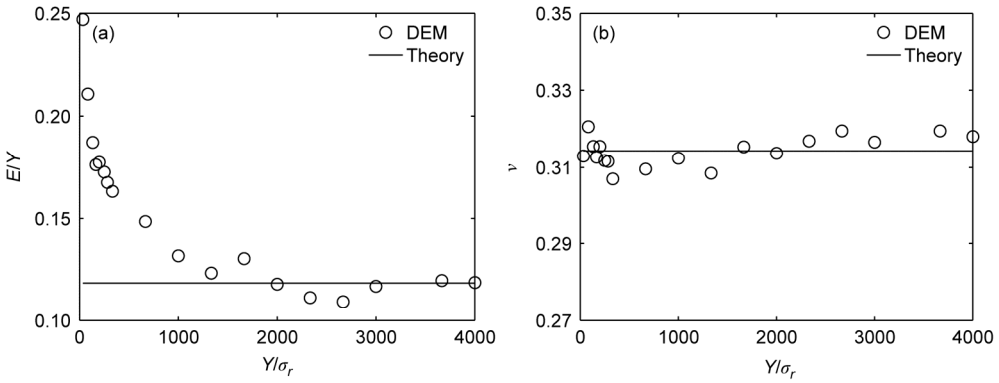

Figure 6 Influence of the stiffness number on the elastic properties of Chende sand. (a) Young's modulus; (b) Poisson's ratio. Here other parameters are α= 0.1, ϕ=30°, α_r=1.0.

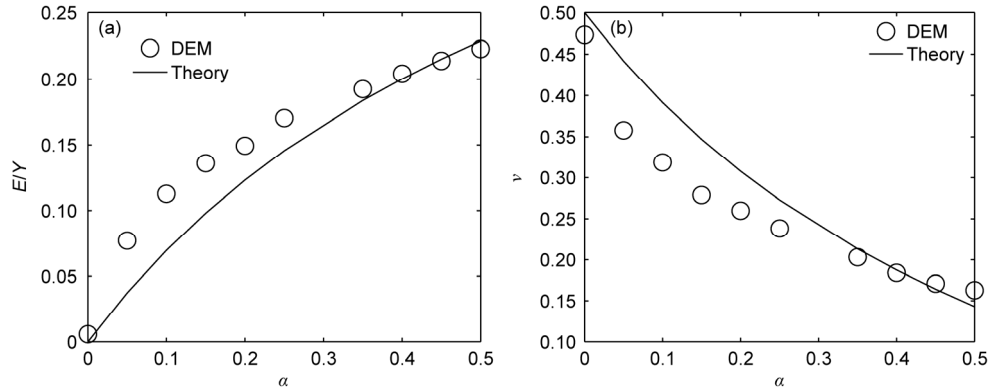

Figure 7 Influence of the stiffness ratio α on the elastic properties of Chende sand. The solid line is Chang's theory. (a) Young's modulus; (b) Poisson's ratio. Other parameters are Y/σ_r = 2700, ϕ=30°, α_r=1.0.

Table 2 Friction angle between different minerals

Mineral	Friction angle (°)
Saturated Quartz	22–24.5
Saturated Feldspar	28–37.6
Saturated Calcite	34.2
Saturated Chlorite	12.4
Kaolinite	12
Illite	10.2
Montmorillonite	4–10

demonstrated in Figure 9 that both peak friction angle and dilatancy angle increase with inter-particle friction angle. Particle contact with a larger inter-particle friction angle exhibits stronger resistance to sliding, so only a larger force is able to force particles to slide. Meanwhile, a larger rotation would happen for particle contact with larger inter-particle friction before sliding happens, which causes a higher dilatancy.

4.4 Influence of the rolling stiffness

The influence of rolling stiffness is examined by varying α_r from 0.01 to 3.0. The response shown in Figure 10 demonstrates that with the increase of rolling stiffness, both peak friction angle and dilatancy angle increase, towards a saturated value as α_r is large, as shown in Figure 11. However, Plassiard's answer that dilatancy is independent of α_r is only a special case. Both particle friction angle and rolling stiffness affect dilatancy angle, but the former is a dominant factor if rolling resistance is large enough, here about 0.5 for Chende sand. Rolling resistance makes it difficult for particles to roll over others, so only a larger force is able to force particles to rotate. The macroscopic effect is to in crease the peak friction angle. As for dilatancy, if the rolling resistance is large enough, then particles can hardly rotate but only slide, which is controlled by inter-particle friction angle, so there is a saturated value of dilatancy.

4.5 Calibration procedure

Based on the above parametric study, we may conclude.

(a) Poisson's ratio depends on stiffness ratio and very little on other parameters.

(b) Young's modulus is proportional to contact modulus and grows with stiffness ratio.

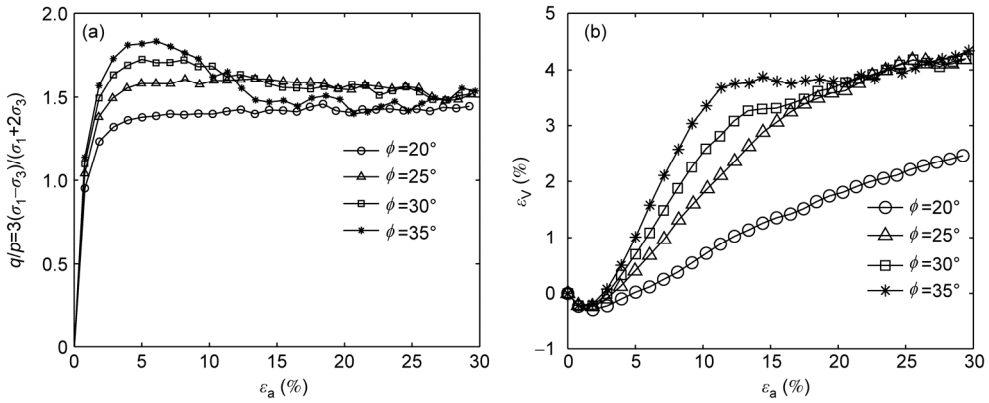

Figure 8 Influences of the particle friction angle on responses of Chende sand. (a) Stress-strain behavior; (b) volume-axial strain behavior. Other parameters are $Y/\sigma_r = 2700$, $\alpha = 0.1$, α_r=1.0.

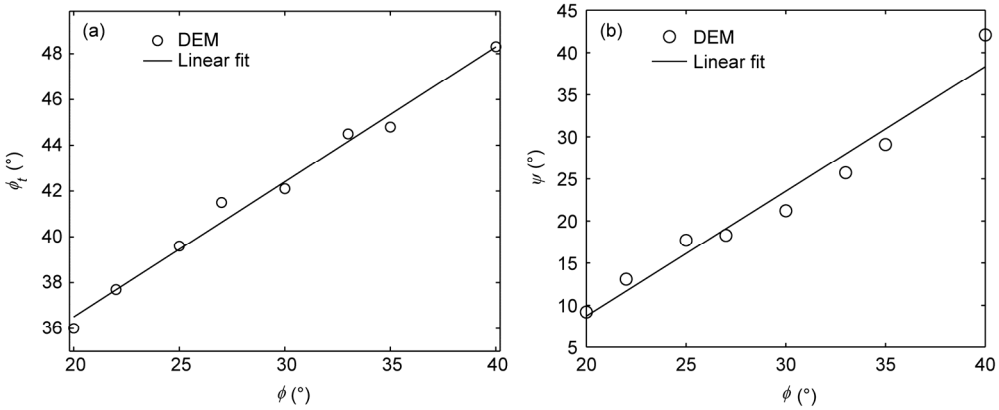

Figure 9 Influence of the inter-particle friction angle on the frictional and dilatant behavior of Chende sand. (a) Peak friction angle; (b) dilatancy angle. Other parameters are $Y/\sigma_r = 2700$, $\alpha = 0.1$, α_r=1.0.

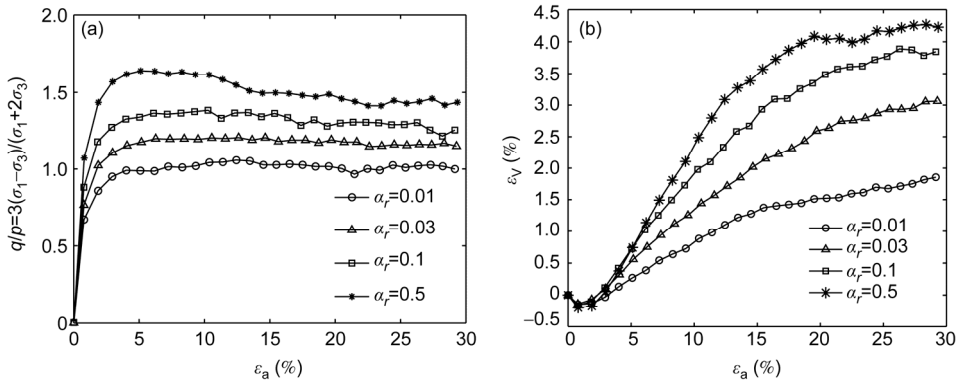

Figure 10 Influence of the rolling stiffness on the responses of Chende sand. (a) Stress-strain curve; (b) volume axial strain curve. Other parameters are $Y/\sigma_r = 2700$, $\alpha = 0.1$, $\phi = 30°$.

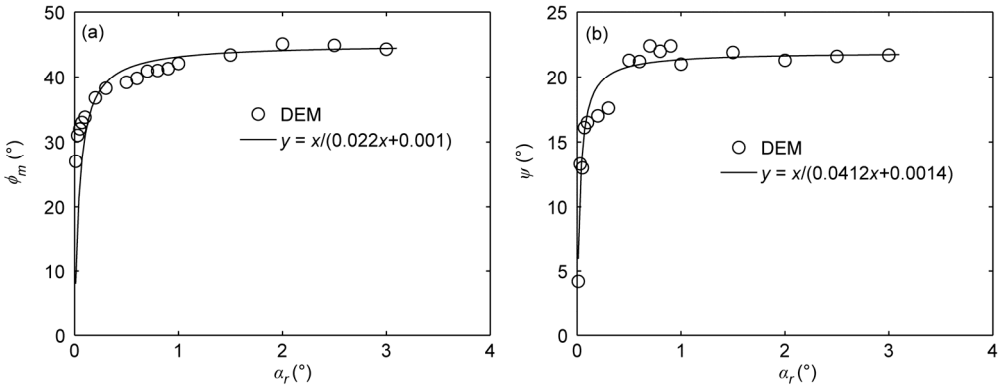

Figure 11 Influence of the rolling stiffness on friction angle (a) and dilatancy angle (b). Other parameters are $Y/\sigma_r = 2700$, $\alpha = 0.1$, $\phi = 30°$.

(c) Peak friction angle of the packing depends on both particle friction angle and rolling stiffness.

(d) Dilatancy angle relies on particle friction and very little on rolling stiffness if rolling stiffness ratio is sufficiently large, for example 0.5 for Chende sand in this study.

Now a calibration procedure for numerical triaxial tests of a real granular material is recommended below.

Firstly, choose an appropriate stiffness ratio so that we can have required Poisson's ratio. Secondly, with stiffness ratio fixed, we start to search for contact modulus by comparing Young's modulus with experiments. Thirdly, we try to find a particle friction angle so that the dilatancy angle is in agreement with experiments. Finally, select a rolling stiffness so that the peak friction angle by DEM is in accord with experiments. Sometimes, one needs to make the calibration by looping between the third and fourth steps.

5 Triaxial compression and extension tests of Chende sand

Chende sand [30] is a uniform sand in the northern part of China, whose physical properties are listed in Table 3.

Table 3 Physical properties of Chende sand

Item	d_{50} (mm)	d_{60}/d_{10}	ρ (kg/m^3)	e_{max}	e_{min}
Value	0.18	2.8	2.63	0.8	0.4

A dense sample corresponding to a relative density of 64% is prepared by radius expansion method. Calibration is performed according to the procedure stated in sect. 4.5, the microscopic parameters are obtained, as shown in Table 1. The calibration procedure is taken step by step for confining stress of 300 kPa. Then with parameters in Table 1, a series of triaxial compression tests were conducted under different confining pressures 100, 300 and 500 kPa, the responses of which are plotted in Figures 3, 12 and 13. The systematic comparisons of the results of the numerical triaxial apparatus and experiments further prove that the DEM model we proposed can serve as a useful tool to obtain macroscopic behaviors of granular materials based on the micromechanics simulation.

Under lateral stress 100 kPa, the response of stress-strain of DEM model is shown in Figure 3(a), together with the experimental results. The peak friction angles of both, 37.5° for DEM model and 36.2° for experiment, are very close, while Young's modulus of DEM model is a bit larger than

the experimental results. In Figure 3(b), the volume-axial strain response is also close to the experimental one and the corresponding dilatancy angles are 9.7° and 12.8°, respectively.

Under lateral stress 300 kPa, Stress-strain response is in accord with experimental results as indicated in Figure 12(a), including the Young's modulus and peak friction angle. Figure 12(b) indicates that DEM model is able to simulate dilatancy quantitatively, with dilatancy angles of DEM model and experiments being 9.4° and 10.1°, respectively.

When a higher confining pressure 500 kPa is applied, the corresponding response is shown in Figure 13. Different from the former cases, Young's modulus by DEM is a bit larger than experiments, but peak friction angles, 35.6° for DEM model and 34.7° for experiment, still agree with each other. As for dilatancy, the DEM model is 8.0° whereas that of experiment is 9.7°.

Figure 14 shows the Mohr circles at the stage of peak stress of experimental results (Figure 14(a)) and DEM model (Figure 14(b)). And the mean friction angles are 35.3° and 36.2° for the experiment and DEM, respectively.

Then based on the calibrated DEM model, triaxial extension tests were performed under lateral confining stress 100, 300 and 500 kPa. After isotropic compression, the two axial plates were moved outward very slowly. Shear stress rises to a peak value very fast with extension, while the volume keeps expanding during the whole triaxial extension tests as shown in Figure 15. The major difference between triaxial compression and extension is the increase or the decrease in mean pressure respectively, which is responsible for initial volume contraction or no contraction. Confining stress plays an opposite role in preserving the internal structure in triaxial compression and extension. Consequently, the influence of confining stress is contrary for dilatancy as shown in Figures 12(b), 13(b) and 15(b).

6 Conclusions

A numerical triaxial apparatus based on discrete element method (DEM) with rolling effect taken into account is developed in this study to examine the mechanical behaviors of nonspherical granular materials at particle level. Based on this rolling resistance model, we have recommended a calibration procedure for cohesionless soil, which was at once applied to the simulation of Chende sand using a series of triaxial compression and extension tests. The responses

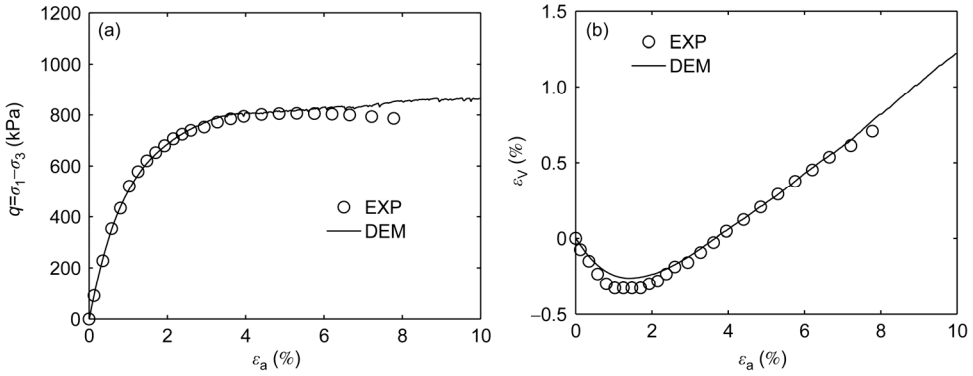

Figure 12 Comparison of numerical and experimental triaxial compression tests for Chende sand. (a) Stress-strain behavior; (b) volume-axial strain response. The lateral stress is 300 kPa.

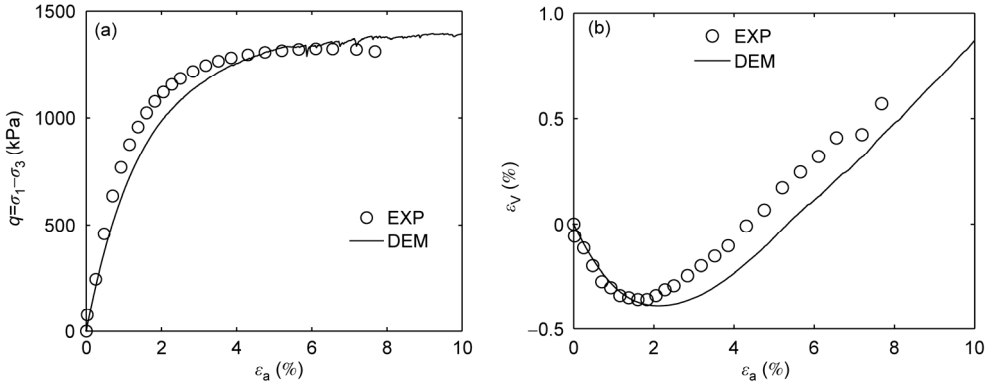

Figure 13 Comparison of numerical and experimental triaxial compression tests for Chende sand. (a) Stress-strain behavior; (b) volume-axial strain response. The lateral stress is 500 kPa.

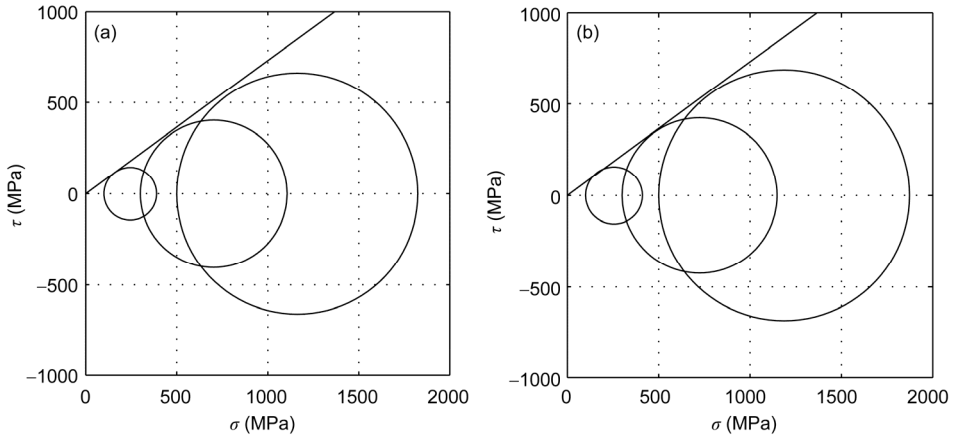

Figure 14 Mohr circles of stress states when Chende sand fails. (a) Experiment; (b) DEM. The lateral stresses of the three Mohr circles are 100, 300 and 500 kPa, respectively.

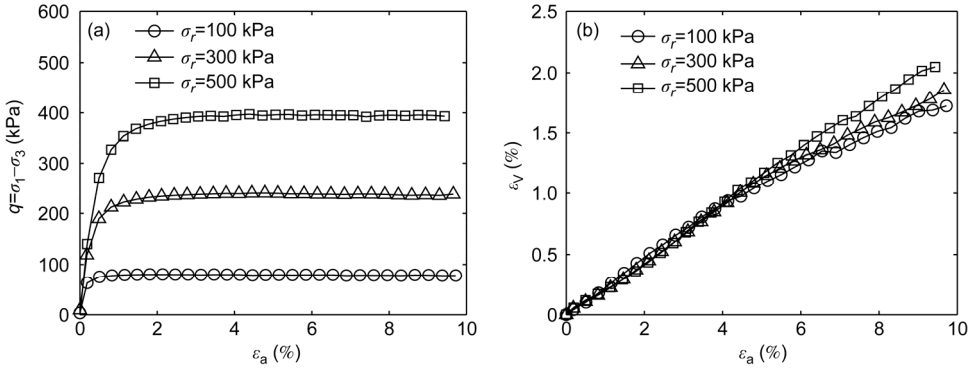

Figure 15 DEM simulation of the triaxial extension of Chende sand under different confining pressures: (a) Stress strain behavior; (b) volume-axial strain response.

of the DEM model are shown in quantitative agreement with experiments.

Dimensional analysis of granular materials demonstrates that four major dimensionless parameters govern their macroscopic behavior so that the elucidation of implied mechanism by relating macroscopic and mesoscopic parameters can be performed. Based on a series of parameter studies, we can finally come to the following conclusions:

(1) Poisson's ratio is essentially controlled by stiffness ratio, very close to the micromechanical model.

(2) Young's modulus is proportional to contact stiffness and grows with stiffness ratio, which exhibits a similar trend to the micromechanical model.

(3) Inter-particles friction angle is the major factor of dilatancy angle if rolling stiffness coefficient is sufficiently large, for example 0.5 for Chende sand in this study.

(4) Peak friction angle relies on both inter-particle friction angle and rolling stiffness.

However, there are still some defects for this DEM model, such as the deviated prediction of Young's modulus and poor ability in simulating softening behavior, so the rolling resistance model still needs further improvement. In addition, liquid bridge effects between particles will be considered and incorporated into the current DEM model to enhance the understanding of the influence of water content on the strength of granular material [2] in the near future.

This work was supported by the National Natural Science Foundation of China (Grant Nos. 11432015 and 10932012). The first author also wants to acknowledge Chareyre et al. for the discussion on mechanics of granular materials on YADE launchpad. We also wish to thank the reviewers for their kind comments and suggestions.

1 Lignon S, Laouafa F, Prunier F, et al. Hydro-mechanical modelling of landslides with a material instability criterion. Geotechnique, 2009, 59(6): 513–524
2 Fu Z, Li J. Strength softening models of soil and its application in rainfall-induced landslide simulation. Theor Appl Mech Lett, 2013, 3(4): 042002
3 Cundall P A, Strack O D L. A discrete numerical model for granular assemblies. Geotechnique, 1979, 29(1): 47–65
4 Ng T T. Particle shape effect on macro- and micro-behaviors of monodisperse ellipsoids. Int J Numer Anal Methods Geomech, 2009, 33(4): 511–527
5 Salot C, Gotteland P, Villard P. Influence of relative density on granular materials behavior: DEM simulations of triaxial tests. Granular Matter, 2009, 11(4): 221–236

6 Azéma E, Radjai F, Saussine G. Quasistatic rheology, force transmission and fabric properties of a packing of irregular polyhedral particles. Mech Mater, 2009, 41(6): 729–741
7 Ji S. Probability analysis of contact forces in quasi-solid-liquid phase transition of granular shear flow. Sci China-Phys Mech Astron, 2013, 56(2): 395–403
8 O'Sullivan C. Particulate Discrete Element Modelling: A Geomechanics Perspective. New York: Taylor & Francis, 2011. 449–494
9 Thornton C. Numerical simulation of deviatoric shear deformation of granular media. Géotechnique, 2000, 50(1): 43–53
10 Jiang M J, Leroueil S, Konrad J M. Insight into strength functions in unsaturated granulate by DEM analysis. Comput Geotech, 2004, 31(6): 473–489
11 Wang Y H, Leung S C. A particulate scale investigation of cemented sand behaviour. Canadian Geotech J, 2008, 45(1): 29–44
12 Utili S, Nova R. DEM analysis of bonded granular geomaterials. Int J Numer Anal Methods Geomech, 2008, 32(17): 1997–2031
13 Jiang M J, Yan H B, Zhu H H, et al. Modeling shear behaviour and strain localization in cemented sands by two-dimensional distinct element method analyses. Comput Geotech, 2011, 38(1): 14–29
14 Jiang M J, Yu H S, Harris D. Bond rolling resistance and its effect on yielding of bonded granulates by DEM analyses. Int J Numer Anal Methods Geomech, 2006, 30(8): 723–761
15 Jiang M J, Yin Z Y. Analysis of stress redistribution in soil and earth pressure on tunnel lining using the discrete element method. Tunnelling Underground Space Tech, 2012, 32: 251–259
16 Mitchell J K, Soga K. Fundamentals of Soil Behavior. New York: Wiley, 2005. 87–91
17 Radjai F, Dubois F. Discrete-element Model of Granular Materials. New York: Wiley, 2011. 123–124
18 Mollon G, Zhao J. Fourier–voronoi-based generation of realistic samples for discrete modelling of granular materials. Granular Matter, 2012, 14(5): 621–638
19 Iwashita K. Mechanics of Granular Materials: An Introduction. Rotterdam: Taylor & Francis, 1999. 178–183
20 Iwashita K, Oda M. Rolling resistance at contacts in simulation of shear band development by dem. J Eng Mech, 1998, 124(3): 285–292
21 Iwashita K, Oda M. Micro-deformation mechanism of shear banding process based on modified distinct element method. Powder Technol, 2000, 109(1): 192–205
22 Jiang M, Yu H S, Harris D. A novel discrete model for granular material incorporating rolling resistance. Comput Geotech, 2005, 32(5): 340–357
23 Wang D, Zhou Y. Discrete element simulation of localized deformation in stochastic distributed granular materials. Sci China Ser G-Phys Mech Astron, 2008, 51(9): 1403–1415
24 Plassiard J P, Belheine N, Donze F V. A spherical discrete element model: Calibration procedure and incremental response. Granular Matter, 2009, 11(5): 293–306
25 Belheine N, Plasslard J P, Donze F V, et al. Numerical simulation of drained triaxial test using 3d discrete element modeling. Comput Geotech, 2009, 36(1-2): 320–331
26 Duriez J, Darve F, Donze F V. A discrete modeling-based constitutive relation for infilled rock joints. Int J Rock Mech Mining Sci, 2011, 48(3): 458–468
27 Scholtès L, Donzé F V, Khanal M. Scale effects on strength of geomaterials, case study: Coal. J Mech Phys Solids, 2011, 59(5): 1131–1146
28 Estrada N, Taboada A, Radjaï F. Shear strength and force transmission in granular media with rolling resistance. Phys Rev E, 2008, 78(2): 021301
29 Šmilauer V, Catalano E, Chareyre B, et al. Yade Documentation. The Yade Project (http://yade-dem org/doc/), 2010
30 Li G X. 3d Constitutive Relationships for Soils and Experiment Validation (in Chinese). Dissertation for Doctoral Degree. Beijing: Tsinghua University, 1985. 34–43
31 Liao C L, Chang T P, Young D H, et al. Stress-strain relationship for granular materials based on the hypothesis of best fit. Int J Solids Struct, 1997, 34(31-32): 4087–4100
32 PFC3D UsM. Itasca Consulting Group. Inc, Minneapolis, USA, 2005
33 Kozicki J, Donze F V. Yade-open dem: An open-source software using a discrete element method to simulate granular material. Eng Comput, 2009, 26(7-8): 786–805
34 Weatherley D. Esys-particle v2. 0 User's Guide. 2009
35 Scholtès L, Chareyre B, Nicot F, et al. Micromechanics of granular materials with capillary effects. Int J Eng Sci, 2009, 47(1): 64–75
36 Wang X L, Li J C. Numerical triaxial apparatus and application. Appl Mech Mater, 2013, 353: 3251–3255
37 Voivret C, Radjai F, Delenne J Y, et al. Space-filling properties of polydisperse granular media. Phys Rev E, 2007, 76(2): 021301
38 Agnolin I, Roux J N. Internal states of model isotropic granular packings. I. Assembling process, geometry, and contact networks. Phys Rev E, 2007, 76(6): 061302
39 Jiang M J, Konrad J M, Leroueil S. An efficient technique for generating homogeneous specimens for DEM studies. Comput Geotech, 2003, 30(7): 579–597
40 Chareyre B, Villard P. Discrete element modeling of curved geosynthetic anchorages with known macro-properties. J Eng Mech-ASCE, 2005, 131(7): 197–203
41 Gilabert F A, Roux J N, Castellanos A. Computer simulation of model cohesive powders: Influence of assembling procedure and contact laws on low consolidation states. Phys Rev E, 2007, 75(1): 011303
42 Tan Q M. Dimensional Analysis: With Case Studies in Mechanics. Heidelberg: Springer, 2011. 7–16
43 Jop P, Forterre Y, Pouliquen O. A constitutive law for dense granular flows. Nature, 2006, 441(7094): 727–730
44 MiDi GDR. On dense granular flows. Eur Phys J E, 2004, 14(4): 341–365
45 Hicher P Y, Chang C S. Evaluation of two homogenization techniques for modeling the elastic behavior of granular materials. J Eng Mech-ASCE, 2005, 131(11): 1184–1194
46 Cambou B, Jean M, Radjaï F. Micromechanics of Granular Materials. London: Wiley Online Library, 2009. 101–147
47 Chang C S, Liao C L. Estimates of elastic modulus for media of randomly packed granules. Appl Mech Rev, 1994, 47(1): 197–206
48 Li G X. Advanced Soil Mechanics (in Chinese). Beijing: Tsing University Press, 2004. 117–119